

**Density-dependent exciton kinetics in synthetic diamond crystals**

N. Naka\*

*Department of Physics, Graduate School of Science, Kyoto University, Kitashirakawa, Sakyo-ku, Kyoto 606-8502, Japan  
and PRESTO, JST, 4-1-8 Honcho Kawaguchi, Saitama 332-0012, Japan*

J. Omachi

*Department of Applied Physics, Graduate School of Engineering, The University of Tokyo, Bunkyo-ku, Tokyo 113-8656, Japan*

H. Sumiya

*Electronics and Materials R&D Laboratories, Sumitomo Electric Industries, 1-1-1 Koyakita, Itami 664-0016, Japan*

K. Tamasaku and T. Ishikawa

*RIKEN SPring-8 Center, 1-1-1 Kouto, Sayo-cho, Sayo-gun, Hyogo 679-5148, Japan*

M. Kuwata-Gonokami†

*Department of Applied Physics, Graduate School of Engineering, The University of Tokyo, Bunkyo-ku, Tokyo 113-8656, Japan  
Photon Science Center, The University of Tokyo, and CREST, JST, 7-3-1 Hongo, Bunkyo-ku, Tokyo 113-8656, Japan*

(Received 21 March 2009; revised manuscript received 8 June 2009; published 7 July 2009)

We have measured transients of excitonic luminescence under pulsed excitation of single-crystal diamond, synthesized by a high-temperature high-pressure method. The longest decay time of 80 ns is measured at a lattice temperature around 100 K in nondoped samples. The decay kinetics strongly depends on the excitation power density and the impurity concentration. Based on the impurity concentrations determined from infrared and ultraviolet absorption coefficients, we simulate the carrier kinetics by solving rate equations for free and bound exciton densities. It is found that annihilation of free excitons via capture to impurity sites and via collection to electron-hole droplets plays an important role at low temperatures.

DOI: [10.1103/PhysRevB.80.035201](https://doi.org/10.1103/PhysRevB.80.035201)

PACS number(s): 71.35.-y, 71.55.-i, 81.05.Uw

**I. INTRODUCTION**

Diamond is a unique material having extreme mechanical hardness, high thermal conductivity, and a wide energy gap located in the deep ultraviolet (UV) spectral region. Recent progress in synthesis techniques provides new application of high-quality diamond crystals for optical windows, crystal monochromators, and high-pressure anvils in addition to conventional uses such as cutting tools and wear-resistance tools.<sup>1</sup> Such diamond crystals also provide an opportunity to obtain deep UV light using edge emission.<sup>2</sup> It is also possible to observe strain-induced effect on the emission properties in the deep UV region.<sup>3,4</sup> In high-purity single crystals of diamond, phonon-assisted recombination of free excitons dominates the edge emission. However, there are only a few reports<sup>5</sup> on the lifetime of free excitons. This is mainly because of the difficulty in preparing pulsed laser light for optical excitation of free excitons.

In previous papers,<sup>6,7</sup> we reported on the formation dynamics of electron-hole droplets (EHDs) in diamond, following excitation by femtosecond laser pulses. It was revealed that electron-hole droplets decay in a few nanosecond, while the free excitons survive much longer. In this study, we measure transients of free excitons in a nanosecond time scale. When the excitation density is so high that electron-hole droplets are created, their formation also affects the kinetics of free excitons, leading to density-dependent kinetics. Therefore, we systematically investigate the density dependence of the transients up to a photon density of  $10^{19}$  cm<sup>-3</sup>.

The interaction between free excitons and impurities is also of importance in describing exciton kinetics. Previous

papers on diamond,<sup>5</sup> silicon,<sup>8,9</sup> and GaAs quantum wells<sup>10</sup> dealt with exciton-impurity interactions in the low-density limit. With a state-of-the-art growth technique, diamond crystals with an impurity concentration as low as  $10^{15}$  cm<sup>-3</sup> are now available.<sup>11</sup> In such samples, the assumption of the absence of saturation in impurity sites becomes invalid. Therefore, we study the doping effect on the decay time of free exciton luminescence using samples containing nitrogen or boron as impurities and expand the discussion for a high-density excitation regime where saturation and nonlinear effects can occur.

**II. EXPERIMENTS**

The samples used were synthesized by the temperature gradient method under high pressure and high temperature using iron-cobalt system solvent with the addition of titanium.<sup>12</sup> The concentration of nitrogen was adjusted by changing the amount of titanium as nitrogen getter added to the solvent. The concentration of boron was controlled by changing the amount of boron contained in the starting material of carbon source. We investigated five samples named S1, S1', S2, S3, and S3'. S2 looks pale blue due to doping with boron, while others are colorless. The impurity concentrations are estimated based on the UV and infrared-absorption coefficients. For a nitrogen concentration  $N_N$ , we use the relation

$$0.56\alpha_N[\text{cm}^{-1}] = N_N[\text{ppm}], \quad (1)$$

where  $\alpha_N$  is the maximum coefficient of the absorption peak at 270 nm. This relation was established by comparison of

TABLE I. Impurity concentrations in respective samples. “–” means that the concentration is lower than the detection limit, which is 0.02 ppm for boron and 0.1 ppm for nitrogen. 1 ppm corresponds to  $1.763 \times 10^{17} \text{ cm}^{-3}$ .

| Sample name | $N_B(n_B)$  | $N_N(n_N)$  |
|-------------|---|---|
| S1          | –   | –   |
| S1'         | –   | –   |
| S2          | 0.25 ppm ( $4.5 \times 10^{16} \text{ cm}^{-3}$ ) | –   |
| S3          | –   | 0.86 ppm ( $1.5 \times 10^{17} \text{ cm}^{-3}$ ) |
| S3'         | –   | 0.40 ppm ( $7.1 \times 10^{16} \text{ cm}^{-3}$ ) |

$\alpha_N$  to the electron-spin-resonance data.<sup>12</sup> For determining boron concentrations, we used a formula derived from Fig. 3 of Ref. 13,

$$4.54A_B[\text{eV cm}^{-1}] = N_B[\text{ppm}], \quad (2)$$

where  $A_B$  is the integral absorption of the peak at  $2800 \text{ cm}^{-1}$ . It is found that S2 contains  $0.05 \pm 0.01$  ppm boron in the central part of the crystal and 0.25 ppm boron in the off-center parts. The data shown below were taken in an off-center part of the crystal. S3 and S3' contain 0.86 and 0.40 ppm nitrogen, respectively. Other concentrations, including those in S1 and S1', are lower than our limit of detection. The detection limit, defined as three times the standard deviation of background, is 0.02 ppm for boron and 0.1 ppm for nitrogen. The impurity concentrations in the samples are summarized in Table I. Also shown in parentheses are impurity concentrations,  $n_B$  and  $n_N$ , in units of  $\text{cm}^{-3}$ . In the following, we show optical data obtained with S1, S2, and S3 only, because S1 and S1' or S3 and S3' displayed essentially the same features.

For photoluminescence and decay measurements, we prepared subpicosecond laser pulses at a wavelength of 214 nm. The fundamental pulses (1 kHz, 900 mW) from a regenerative amplified Ti:sapphire laser (Clark MXR Inc., CPA2010) is directed to a nonlinear parametric amplification system (Light Conversion Ltd., TOPAS). The signal light is at a wavelength of  $1.28 \mu\text{m}$  and the power is 60 mW. The frequency-unconverted portion of the fundamental light through the TOPAS is converted to the third harmonics of  $\sim 10$  mW at a wavelength of 257 nm, by using two  $\beta\text{-BaB}_2\text{O}_4$  crystals. Next we take the sum frequency of the third harmonics and the signal light to obtain final pulses of 4 mW at the wavelength of 214 nm.

The samples are mounted on a copper block attached to the cold finger of a closed-cycle cryostat. The temperature is monitored by a thermocouple mounted on the block. The laser light is focused on a sample surface by a  $\text{CaF}_2$  lens of  $f=10$  cm. The spot size was measured and found to be  $34 \pm 2 \mu\text{m}$  by the knife-edge method. The photon energy of the laser light is above the indirect gap of diamond, 5.49 eV. Following the one-photon absorption process, the photogenerated carriers thermalize to the conduction valleys and form indirect excitons and electron-hole droplets.<sup>6</sup> The luminescence from the sample is reflected by a dichroic mirror which cuts off the scattering light of the third harmonics and projected onto the entrance slit of a 50 cm monochromator

(Acton Research Co., SP500) by an achromatic lens. The signal is detected by a nitrogen-cooled charge-coupled-device camera or a photomultiplier (Hamamatsu, R1477). For decay measurements, the signal from the photomultiplier is sent to an oscilloscope (Tektronics, TDS744A) triggered by the switching voltage of the Pockels cell in the laser cavity.

### III. RESULTS AND DISCUSSION

#### A. Photoluminescence spectra

Figure 1(a) shows photoluminescence spectra of S1 at various temperatures. The red (light gray in print), blue (gray), and black lines correspond to excitation densities of 50, 5, and  $0.5 \text{ mJ/cm}^2$ , respectively. Hereafter, we use the same color codes through all the figures. The strongest peak around the photon energy of 5.27 eV is due to transverse-optical (TO)-phonon-assisted recombination of free excitons. We denote this line as FE(TO). The linewidth shows broadening with increasing temperature, reflecting the thermal distribution of free excitons in the momentum space. The shoulder at the high-energy tail is due to transverse acoustic (TA)-phonon-assisted recombination, FE(TA). The small peak around 5.12 eV is due to two-phonon-assisted recombination of free excitons, FE(TO- $\text{O}_\Gamma$ ), involving TO and zone center optical ( $\text{O}_\Gamma$ ) phonons. A broad structure centered around 5.17 eV is seen below 80 K, as marked by arrows in the figure. It is due to TO-phonon-assisted recombination of EHDs which appears at a high-excitation density.

Figure 1(b) is a similar plot for S2 containing 0.25 ppm boron. TO, TA, and TO- $\text{O}_\Gamma$  phonon-assisted recombination lines of free excitons are seen as in S1. The broad peak seen above 120 K is not due to EHDs but due to plasma. The broad peak seen below 80 K is due to phonon-assisted recombination of EHDs. The overall intensity of the photoluminescence is about one order of magnitude weaker than in S1, but the relative intensities of the EHDs to excitonic lines are stronger. In general, formation mechanisms of EHDs are classified as homogeneous and inhomogeneous nucleations.<sup>14</sup> A homogeneous nucleation occurs in a free exciton gas, while an inhomogeneous one starts at some defects acting as nucleation centers. The enhancement of the EHD luminescence in S2 implies that nucleation of EHDs is triggered at impurity sites, and that inhomogeneous nucleation dominates over homogeneous nucleation. In addition to the EHD line, there is a small doublet peak around 5.23 eV.

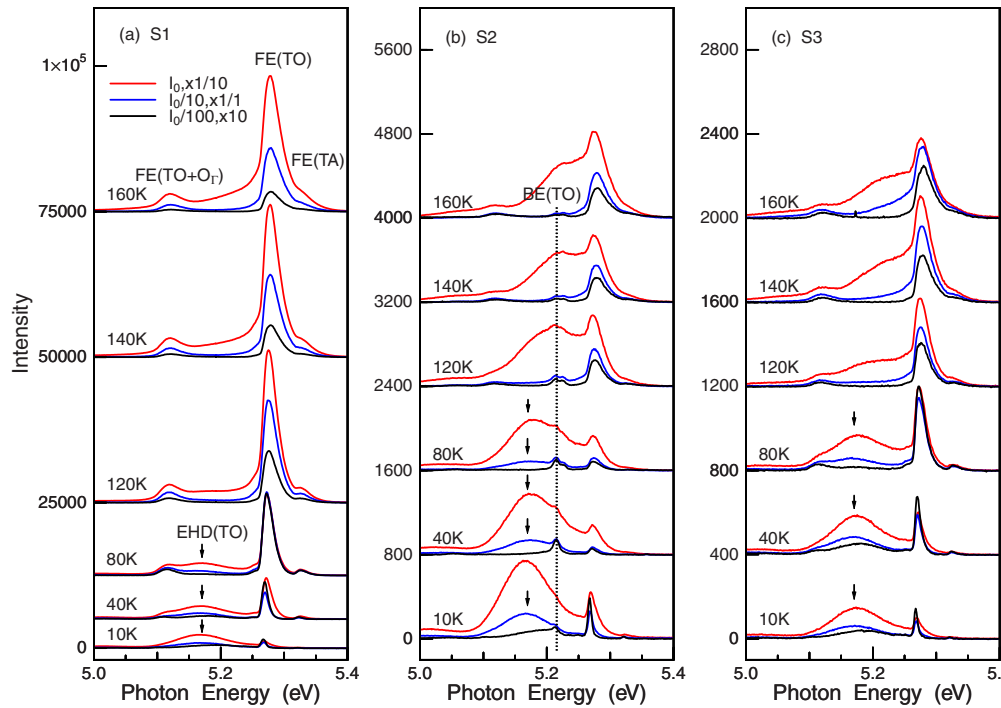


FIG. 1. (Color online) Spectra of edge emission in diamond. Red (light gray in print), blue (gray), and black lines correspond to excitation densities of 50, 5, and 0.5  $\text{mJ}/\text{cm}^2$ , respectively. The lattice temperatures are indicated near the spectra. The base lines have been displaced for clarity. (a) S1 with  $<0.1$  ppm nitrogen and  $<0.02$  ppm boron. FE(X) denotes recombination of free excitons accompanying emission of phonons of X mode. Arrows indicate TO-phonon-assisted recombination of EHDs. (b) S2 containing 0.25 ppm boron. BE(TO) means TO-phonon-assisted recombination of excitons bound to boron sites. (c) S3 containing 0.86 ppm nitrogen.

It is due to TO-phonon-assisted recombination of excitons bound to boron sites, BE(TO).<sup>15</sup> The intensity ratio,  $\sim 1$  at 80 K, of the BE line to the FE line implies a boron concentration of 0.5 ppm according to a report on cathodoluminescence.<sup>16</sup> This value is higher than the one extracted from our absorption measurement. The disagreement is likely due to the saturation of the BE(TO) intensity under pulsed excitation or due to difference in the excitation configuration (i.e., surface excitation for luminescence and bulk detection for absorption).

Figure 1(c) shows luminescence spectra obtained with S3. The overall temperature dependence is similar to that in S2, except for the absence of the bound exciton line. The ratio of EHD to the free exciton lines is again larger than in S1, indicating inhomogeneous nucleation starting at nitrogen sites. The overall luminescence intensity in S3 is even smaller than in S2. This is consistent with the higher concentration of impurities in S3 than in S2. Most of the free excitons are captured at nitrogen sites and then nonradiatively recombine.

### B. Density dependence and doping effects

Figure 2(a) shows representative decay curves of phonon-assisted recombination of free excitons, FE(TO), in S1 at 140 K. The red (light gray in print), blue (gray), and black lines correspond to excitation densities of 50, 5, and 0.5  $\text{mJ}/\text{cm}^2$ , respectively. It is found that the decay time of the luminescence strongly depends on the excitation density. Namely, the decay slows down with increasing density and reaches to

a value on the order of 100 ns for the highest excitation density. Figure 2(b) shows decay curves of FE(TO) in S2. The free exciton luminescence decays much faster than in S1. The  $1/e$  times are shorter than 10 ns for every excitation density. The dashed line in Fig. 2(b) is a decay curve of bound exciton luminescence, BE(TO), in S2 at 80 K. The decay curve was taken under a weak excitation of 0.5  $\text{mJ}/\text{cm}^2$  in order to avoid the spectral overlap with EHD(TO). The decay time was found to be less than 1 ns, which was limited by our temporal resolution. Although not shown in the figure, S3 has a decay time shorter than 10 ns.

In order to understand the density dependence and the drastic shortening of the decay time by doping, we assume a two-level system consisting of free and bound exciton states. We take a set of rate equations for free and bound exciton

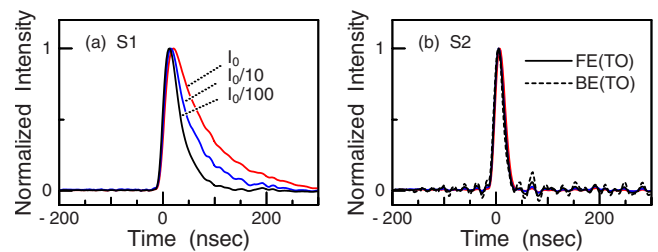


FIG. 2. (Color online) (a) Decay curves of TO-phonon-assisted recombination of free excitons at different excitation powers, obtained with S1 at 140 K.  $I_0=50$   $\text{mJ}/\text{cm}^2$ . (b) Decay curves of free excitons obtained with S2 at 140 K. The dashed line is a decay curve of bound excitons obtained with S2 at 80 K.

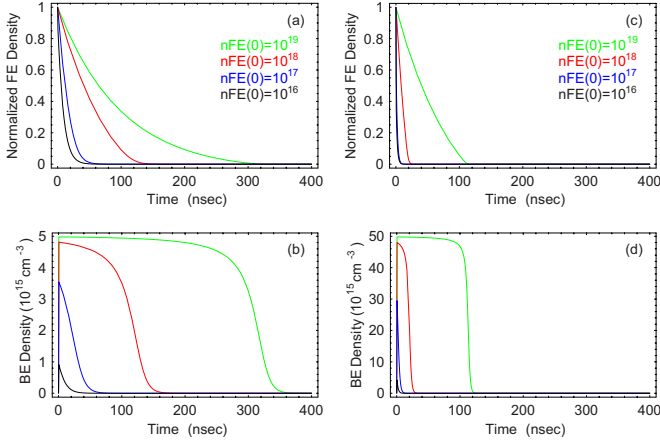


FIG. 3. (Color online) Transients obtained by solving Eqs. (3) and (4). Temporal change in (a)  $n_{\text{FE}}$  with  $n_i = 5 \times 10^{15} \text{ cm}^{-3}$ , (b)  $n_{\text{BE}}$  with  $n_i = 5 \times 10^{15} \text{ cm}^{-3}$ , (c)  $n_{\text{FE}}$  with  $n_i = 5 \times 10^{16} \text{ cm}^{-3}$ , and (d)  $n_{\text{BE}}$  with  $n_i = 5 \times 10^{16} \text{ cm}^{-3}$ . The initial free exciton density was assumed as  $n_{\text{FE}}(0) = 10^{19}, 10^{18}, 10^{17}$ , and  $10^{16} \text{ cm}^{-3}$ , from upper to lower curves.

densities,  $n_{\text{FE}}(t), n_{\text{BE}}(t)$ , as in Ref. 10 as follows:

$$\frac{dn_{\text{FE}}}{dt} = -\frac{n_{\text{FE}}}{t_{\text{FE}}} - Cn_{\text{FE}}(n_i - n_{\text{BE}}) + Rn_{\text{BE}}, \quad (3)$$

$$\frac{dn_{\text{BE}}}{dt} = -\frac{n_{\text{BE}}}{t_{\text{BE}}} + Cn_{\text{FE}}(n_i - n_{\text{BE}}) - Rn_{\text{BE}}. \quad (4)$$

Here,  $t_{\text{FE}}$  is the decay time of free exciton population and  $t_{\text{BE}}$  is the decay time of bound exciton population. The second term in the right-hand sides of Eqs. (3) and (4) represent the capture of free excitons to impurity sites. The capture rate is proportional to the free exciton density  $n_{\text{FE}}$  and the density  $(n_i - n_{\text{BE}})$  of the available sites, where  $n_i$  is the concentration of impurities. This term is of the second order in density and includes saturation in the number of sites available for capture.  $C$  is the capture rate and  $R$  is the release rate.

Figures 3(a) and 3(b) show simulated transients of free and bound exciton densities, respectively. The parameters are chosen as  $t_{\text{BE}} = 1 \text{ ns}$ ,  $t_{\text{FE}} = 100 \text{ ns}$ ,  $C = 8 \times 10^{-7} \text{ cm}^3 \text{ s}^{-1}$ ,  $R = 3 \times 10^{10} \text{ s}^{-1}$ , and  $n_i = 5 \times 10^{15} \text{ cm}^{-3}$  with an initial condition of  $n_{\text{BE}}(0) = 0$ . The vertical axis is a density normalized by initial population of free excitons, which is assumed as  $n_{\text{FE}}(0) = 10^{19}, 10^{18}, 10^{17}$ , and  $10^{16} \text{ cm}^{-3}$ . The most prominent feature for the free exciton density, i.e., elongation of the decay time up to 100 ns with increasing excitation density is well reproduced. We expect slower decays for the bound exciton density because of the saturation of the available sites at early times. When all the impurity sites are occupied, the bound exciton density stays near  $n_i$  for some temporal range. This occurs under a high-excitation density and is seen as a plateau of  $n_{\text{BE}}$  in Fig. 3(b). In this regime, the left-hand side of Eq. (4) can be replaced with zero, and Eqs. (3) and (4) reduce to a single equation:  $dn_{\text{FE}}/dt = -n_{\text{FE}}/t_{\text{FE}} - n_{\text{BE}}/t_{\text{BE}}$ . Since the free exciton term  $-n_{\text{FE}}/t_{\text{FE}}$  dominates over the time-independent term  $-n_{\text{BE}}/t_{\text{BE}}$ , the free exciton density decays exponentially. Figures 3(c) and 3(d) show

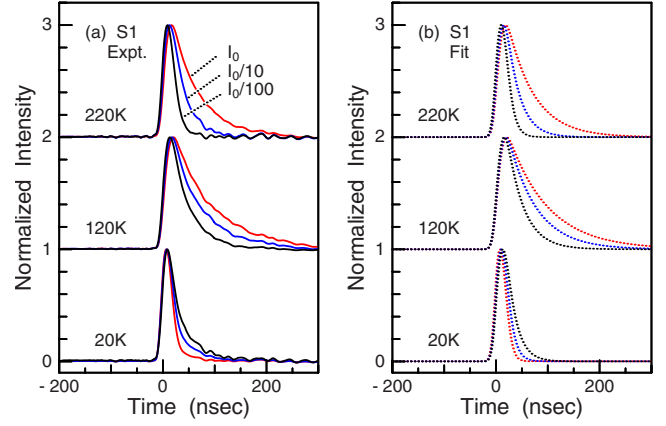


FIG. 4. (Color online) (a) Decay curves of TO-phonon-assisted recombination of free excitons in S1 at different excitation powers and temperatures. The decay kinetics depends both on the power density and temperature.  $I_0 = 50 \text{ mJ/cm}^2$ . (b) Best fits of the decay curves in (a) to a single exponential function.

simulated transients obtained by increasing the density of impurities by a factor of 10,  $n_i = 5 \times 10^{16} \text{ cm}^{-3}$ . The remarkable shortening of the decay time of free and bound exciton densities is reproduced. Therefore, fast decays of the free exciton density can be interpreted as due to capture of free excitons to impurity sites. With this high impurity concentration, the time-independent term  $-n_{\text{BE}}/t_{\text{BE}}$  can dominate over the free exciton term  $-n_{\text{FE}}/t_{\text{FE}}$ . This leads to a free exciton density changing almost linearly with time, as observed in Fig. 3(c).

At this temperature, the collection of excitons to EHDs does not occur because the excitonic temperature is above the critical temperature of formation of EHDs. We take this effect into account in the next section.

### C. Temperature dependence of the decay

In Fig. 4(a), the decay curves of FE(TO) in S1 at different temperatures and excitation densities are shown. We performed single exponential fit and extracted the decay time. The dotted lines in Fig. 4(b) are best fits of the data in Fig. 4(a) to a single exponential decay with convolution by a response function of the detection system. The response function was determined by the temporal response of the system to the scattering light of the third harmonics, which has shorter ( $\sigma = 10 \text{ ns}$ ) and longer ( $\sigma = 15 \text{ ns}$ ) tails into negative and positive delay times. This asymmetric response is due to the running time of amplified electrons in the photomultiplier. The agreement between data and calculation is very good, and a decay time down to 1 ns is resolved although the half-width (full width at half maximum) of the response function is 18 ns.

Figure 5(a) summarizes the temperature dependence of the decay time in S1. The longest decay time was obtained around 100 K for the highest excitation density. For lower excitation densities, the temperature for the longest decay time becomes slightly lower. As pointed out by Takiyama *et al.* in Ref. 5, there is a clear correlation between the decay times and the photoluminescence intensities. To confirm this,

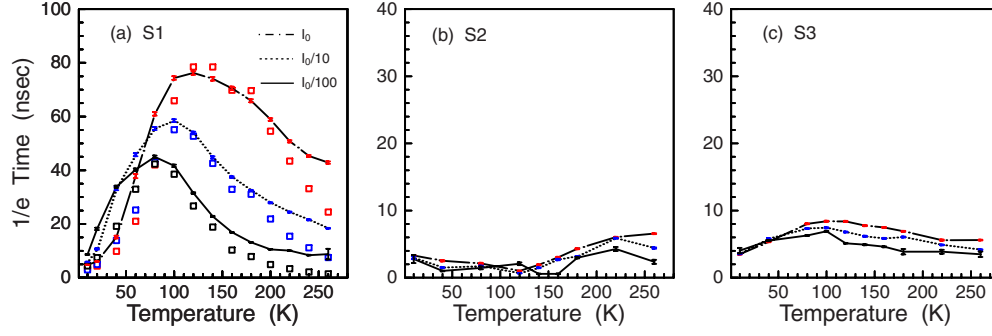


FIG. 5. (Color online) Temperature dependence of the  $1/e$  time obtained from fits to a single exponential decay in (a) S1, (b) S2, and (c) S3. In (a), the intensity of the TO-phonon-assisted recombination of free excitons in S1 is superimposed by squares.

we plot the spectrally integrated intensity of FE(TO) in S1 by squares in Fig. 5(a). In Figs. 5(b) and 5(c), plotted are temperature dependences of the decay time in S2 and S3, respectively. In S2, the decay time is very short at a temperature below 140 K and it becomes slightly longer at higher temperatures. In S3, the decay time has its maximum of  $\sim 10$  ns around 100 K.

In a previous study using nanosecond pulse excitations,<sup>5</sup> a hill-shaped temperature dependence of the decay time was reported. The authors explained the temperature dependence by a formula derived from linearized rate equations for free and bound exciton populations. The shortening of the decay time at high and low temperatures is interpreted as exciton capture to impurities and exciton ionization, respectively. In Ref. 5, the linearization was valid because the exciton density was much lower than the impurity concentration. In our experiments, however, the excitation density is high enough that  $n_{FE}$  can exceed  $n_i$ . The observed strong density dependence also suggests that linearization is valid only for low-density cases. Therefore, without linearization, we introduce temperature-dependent  $t_{FE}$ ,  $C$ , and  $R$  in the coupled equations. The capture rate has a temperature dependence like  $C(T) = 4\sigma_{BE}v$ , where  $\sigma_{BE}$  is the cross section for capture and  $v = \sqrt{k_B T / 2\pi m}$  is the thermal velocity<sup>9</sup> with the total optical mass of excitons,  $m = 0.87m_0$ . The release rate is given by a Richardson-Dushman current between free and bound states separated by an activation energy of  $E_i$ :<sup>9</sup>  $R = C(T)(mk_B T / 2\pi\hbar^2)^{3/2} \exp(-E_i/k_B T)$ . We also take account of the annihilation of excitons due to collection to EHDs in term  $A(T)$ , as described in the Appendix,

$$\frac{dn_{FE}}{dt} = -\frac{n_{FE}}{t_{FE}(T)} - C(T)n_{FE}(n_i - n_{BE}) + R(T)n_{BE} + A(T), \quad (5)$$

$$\frac{dn_{BE}}{dt} = -\frac{n_{BE}}{t_{BE}} + C(T)n_{FE}(n_i - n_{BE}) - R(T)n_{BE}. \quad (6)$$

Including the ionization of excitons at high temperatures, one can express a decay time of free excitons as

$$\frac{1}{t_{FE}(T)} = \frac{1}{t_X} [1 + K \exp(-E_{FE}/k_B T)]. \quad (7)$$

In Eq. (7), we assumed a detailed balance to the ionized state separated by a binding energy of  $E_{FE} = 80$  meV.<sup>15</sup>

With parameters as explained in the Appendix, we numerically solve the coupled rate equations and obtain transients for  $n_{FE}$  and  $n_{BE}$ . The extracted  $1/e$  times corresponding to S1, S2, and S3 are plotted in Figs. 6(a)–6(c), respectively. An assumption that a photon density of  $50$  mJ/cm<sup>2</sup> corresponds to an exciton density of  $10^{18}$  cm<sup>-3</sup> gives a good agreement to the experimental curves in Fig. 5. This means that the exciton density is smaller than 10% of the photon density estimated from the penetration depth of  $15$   $\mu$ m and the measured spot size. The difference can be partly due to diffusion of excitons from the excitation spot or due to conversion efficiency from photons to excitons less than unity. The temperature dependences in S1 and S2 are reproduced by our simulation, just by changing the impurity concentration and assuming different lifetimes for excitons

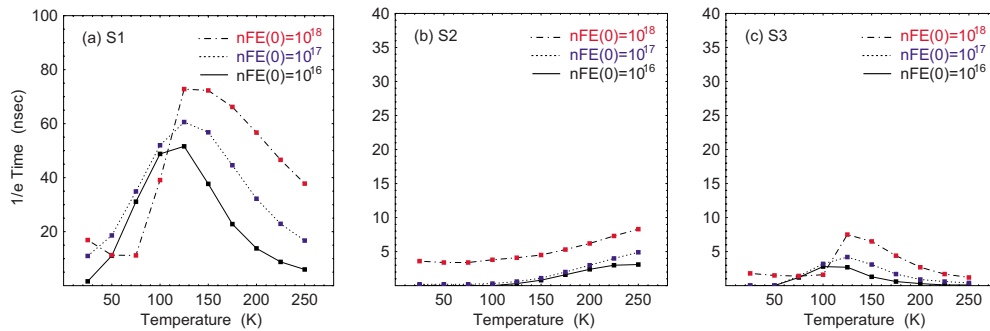


FIG. 6. (Color online) Temperature dependence of the  $1/e$  time extracted from simulated transients. (a)  $K = K_0 \equiv 6.3 \times 10^{10} / \sqrt{n_{FE}(0)}$ ,  $n_N = 5.0 \times 10^{15}$  cm<sup>-3</sup>, and  $\tau_{BE} = 1.0$  ns; (b)  $K = K_0$ ,  $n_B = 4.5 \times 10^{16}$  cm<sup>-3</sup>, and  $\tau_{BE} = 0.3$  ns; and (c)  $K = 50K_0$ ,  $n_N = 1.5 \times 10^{17}$  cm<sup>-3</sup>, and  $\tau_{BE} = 1.0$  ns.

bound at boron (0.3 ns) and at nitrogen (1.0 ns). For S3, we obtained better agreement with a larger value of  $K$ . The decay time in S1 at a temperature below the critical temperature of EHD formation shortens with increasing density because of a faster capture of excitons to EHDs. In S2 the major source of annihilating free excitons is the capture at boron sites; therefore, the decay slows down at higher temperature where the release rate increases. The decay times in S3 around 100 K are slightly longer than in S2 because of the smaller activation energy.

#### IV. CONCLUSION

We have measured transients of excitonic luminescence in nondoped and doped diamond crystals. The longest decay time of 80 ns was measured in nondoped samples at a lattice temperature around 100 K. It is found that the decay time strongly depends on the temperature, the excitation density, and the concentration of the impurities. We model the kinetics of free excitons and of excitons bound to impurity sites. Inclusion of annihilation of free excitons via bound states and collection to electron-hole droplets lead to successful reproduction of the temperature- and density-dependent decay for samples containing different amounts of impurities. The quantitative discussion on the decay channels provides an insight into realizing long-lived high-density excitons in diamond, which is in close connection to the control of quantum phases.<sup>3</sup>

#### ACKNOWLEDGMENTS

We thank J. B. Heroux (The University of Tokyo) for a critical reading of the manuscript. This work was partially supported by the Photon Frontier Network Program of MEXT, KAKENHI (Grant No. 20104002), and by Special Coordination Funds for Promoting Science and Technology from MEXT, Japan.

#### APPENDIX: PARAMETERS USED IN THE SIMULATION

In this appendix, we give a detailed explanation of parameters used in the simulation. To reproduce the high-temperature drop of the decay time, we need to take a density dependent  $K$  in Eq. (7). Phenomenologically we employed

$K \propto n_{\text{FE}}(0)^\beta$  and found that  $\beta \sim -0.5$  best reproduces the data. We determine  $K$  so as a simulated decay best fits to the observed one at high temperatures. The cross section for capture of free excitons to impurity sites is not known. Furthermore, the measured rise in the transients of bound exciton luminescence was too fast to extract the cross section for capture by fitting the transients. Therefore, we assume  $\sigma_{\text{BE}} = 10^{-13} \text{ cm}^2$  as in the case of capture of free excitons at phosphor and boron sites in silicon.<sup>8</sup> With fixed (but density dependent)  $K$  and  $n_i$  determined from absorption measurements, we find activation energies, which best explain the low-temperature drop of the decay time. The activation energies are found as  $E_B = 40$  and  $E_N = 10$  meV. These values differ from the ones estimated from the spectroscopic data:  $E_B = 54$  and  $E_N = 150$  meV. The free exciton lifetime  $t_{\text{FE}}$  was determined so as to reproduce the absolute value of the lifetime at the maximum temperature, after fixing the above parameters which are sensitive to the temperature dependence.

To be accurate, modeling the EHD dynamics needs discrete master equations.<sup>17</sup> However, here we take a rather simplified model for collection of excitons to EHDs:

$$A(T) = n_d \nu^{2/3} 4\sigma_d \nu \left[ -n_{\text{FE}} + \left( \frac{mk_B T}{2\pi\hbar^2} \right)^{3/2} \exp(-E_d/k_B T) \right] \eta(T). \quad (\text{A1})$$

The capture occurs proportionally to the surface area of droplets, which is proportional to  $n_d \nu^{2/3}$ , where  $n_d$  is the number of droplets in a unit volume and  $\nu$  is an averaged number of electron-hole pairs in each droplet.  $E_d = 50$  meV is the binding energy of droplets. For transients of droplets,<sup>14</sup> we assumed  $d\nu/dt = -\nu/t_0 + A(T)/n_d$  with  $n_d = 2 \times 10^{10} \text{ cm}^{-3}$ , and with  $t_0 = 1000$  ps determined from experiments.<sup>6</sup>  $\eta(T)$  accounts for a droplet fraction which varies with temperature. In an open and nonequilibrium system such as electrons and holes in diamond, it is not apparent that the droplet fraction follows a model for a degenerate plasma or empirical formula for a classical gas. As a first approximation, we take the latter after Guggenheim,<sup>18</sup>  $\eta(T) = (2/7)[1 + (3/4)(1 - T/T_c) + (7/4)(1 - T/T_c)^{1/3}]$ , where  $T_c = 100$  K and  $T$  is the lattice temperature.<sup>19</sup> The capture cross section is assumed as  $\sigma_d = \pi \left( \frac{3}{4\pi n_0} \right)^{2/3}$ , where  $n_0 = 10^{20} \text{ cm}^{-3}$  is the density of carriers inside droplets.<sup>17</sup>

\*naka@scphys.kyoto-u.ac.jp

†gonokami@ap.t.u-tokyo.ac.jp

<sup>1</sup>H. Sumiya, N. Toda, and S. Satoh, *New Diamond Front. Carbon Technol.* **10**, 233 (2000).

<sup>2</sup>K. Horiuchi, K. Nakamura, and S. Yamashita, *Jpn. J. Appl. Phys., Part 2* **39**, L604 (2000).

<sup>3</sup>N. Naka, J. Omachi, and M. Kuwata-Gonokami, *Phys. Rev. B* **76**, 193202 (2007).

<sup>4</sup>H. Sumiya, Y. Nakamoto, K. Shimizu, and H. Kanda, *Appl. Phys. Lett.* **93**, 101915 (2008).

<sup>5</sup>K. Takiyama, M. I. Abd-Elrahman, T. Fujita, and T. Oda, *Solid*

*State Commun.* **99**, 793 (1996).

<sup>6</sup>M. Nagai, R. Shimano, K. Horiuchi, and M. Kuwata-Gonokami, *Phys. Rev. B* **68**, 081202(R) (2003).

<sup>7</sup>R. Shimano, M. Nagai, K. Horiuchi, and M. Kuwata-Gonokami, *Phys. Rev. Lett.* **88**, 057404 (2002).

<sup>8</sup>R. B. Hammond and R. N. Silver, *Appl. Phys. Lett.* **36**, 68 (1980).

<sup>9</sup>R. M. Feenstra and T. C. McGill, *Solid State Commun.* **36**, 1039 (1980).

<sup>10</sup>C. I. Harris, B. Monemar, H. Kalt, P. O. Holtz, M. Sundaram, J. L. Merz, and A. C. Gossard, *Phys. Rev. B* **50**, 18367 (1994).

- <sup>11</sup>K. Horiuchi, K. Nakamura, S. Yamashita, and M. Kuwata-Gonokami, *Jpn. J. Appl. Phys., Part 2* **36**, L1505 (1997).
- <sup>12</sup>H. Sumiya and S. Satoh, *Diamond Relat. Mater.* **5**, 1359 (1996).
- <sup>13</sup>A. T. Collins and A. W. S. Williams, *J. Phys. C* **4**, 1789 (1971).
- <sup>14</sup>R. M. Westervelt, in *Electron-Hole Droplets in Semiconductors*, edited by C. D. Jeffries and L. V. Keldysh (North-Holland, Amsterdam, 1983), p. 205.
- <sup>15</sup>P. J. Dean, E. C. Lightowlers, and D. R. Wight, *Phys. Rev.* **140**, A352 (1965).
- <sup>16</sup>H. Kwarada, H. Matsuyama, Y. Yokota, T. Sogi, A. Yamaguchi, and A. Hiraki, *Phys. Rev. B* **47**, 3633 (1993).
- <sup>17</sup>J. H. Jiang, M. W. Wu, M. Nagai, and M. Kuwata-Gonokami, *Phys. Rev. B* **71**, 035215 (2005).
- <sup>18</sup>E. A. Guggenheim, *J. Chem. Phys.* **13**, 253 (1945).
- <sup>19</sup> $T_c=165$  K given in Ref. 7 is not a lattice temperature but a temperature of the electron-hole system.